Targeting novel sodium iodide symporter interactors ADP-ribosylation factor 4 and valosin-containing protein enhances radioiodine uptake

Fletcher, Alice; Read, Martin; Thornton, Caitlin; Larner, Dean; Poole, Vikki; Brookes, Kate; Nieto, Hannah; Alshahrani, Mohammed; Thompson, Rebecca; Lavery, Gareth; Landa, Iñigo; Fagin, James A; Campbell, Moray J; Boelaert, Kristien; Turnell, Andrew; Smith, Vicki; McCabe, Christopher

DOI:
10.1158/0008-5472.CAN-19-1957

Document Version
Peer reviewed version

Citation for published version (Harvard):
Fletcher, A, Read, M, Thornton, C, Larner, D, Poole, V, Brookes, K, Nieto, H, Alshahrani, M, Thompson, R, Lavery, G, Landa, I, Fagin, JA, Campbell, MJ, Boelaert, K, Turnell, A, Smith, V & McCabe, C 2020, 'Targeting novel sodium iodide symporter interactors ADP-ribosylation factor 4 and valosin-containing protein enhances radioiodine uptake', *Cancer Research*, vol. 80, no. 1, pp. 102–115. https://doi.org/10.1158/0008-5472.CAN-19-1957

Targeting novel sodium iodide symporter interactors ADP-ribosylation factor 4 (ARF4) and valosin-containing protein (VCP) enhances radioiodine uptake

Alice Fletcher[1], Martin L. Read[1], Caitlin E.M. Thornton[1], Dean P. Larner[1], Vikki L. Poole[1], Katie Brookes[1], Hannah R. Nieto[1], Mohammed Alshahrani[1], Rebecca J. Thompson[1], Gareth G. Lavery[1], Iñigo Landa[2], James A. Fagin[3], Moray J. Campbell[4], Kristien Boelaert[1], Andrew S. Turnell[5], Vicki E. Smith[1†], Christopher J. McCabe[1*†]

[1]Institute of Metabolism and Systems Research, University of Birmingham, Birmingham, United Kingdom

[2]Human Oncology and Pathogenesis Program, Memorial Sloan Kettering Cancer Center, New York, New York

[3]Department of Medicine, Memorial Sloan Kettering Cancer Center, New York, New York

[4]Division of Pharmaceutics and Pharmaceutical Chemistry, College of Pharmacy, The Ohio State University, Columbus, Ohio, USA

[5]Institute of Cancer and Genomic Sciences, University of Birmingham, Birmingham, United Kingdom

[*]**Corresponding author**: Professor Christopher J. McCabe, Institute of Metabolism and Systems Research, College of Medical and Dental Sciences, University of Birmingham, Birmingham, B15 2TH, UK. Email: mccabcjz@bham.ac.uk; Tel.: +44 (0) 121 415 8713

[†]**Senior authors**

Running title: Targeting NIS interactors to enhance radioiodine uptake

Conflict of Interest: The authors assert they have no conflicts of interest.

ABSTRACT

The sodium iodide symporter (NIS) is required for iodide uptake which facilitates thyroid hormone biosynthesis. NIS has been exploited for over 75 years in ablative radioiodine (RAI) treatment of thyroid cancer where its ability to transport radioisotopes depends on its localization to the plasma membrane. The advent of NIS-based *in vivo* imaging and theranostic strategies in other malignancies and disease modalities has recently increased the clinical importance of NIS. However, NIS trafficking remains ill-defined. Here, we employed tandem mass spectrometry followed by co-immunoprecipitation and proximity ligation assays to identify and validate two key nodes - ADP-ribosylation factor 4 (ARF4) and valosin-containing protein (VCP) - controlling NIS trafficking. Using cell surface biotinylation assays and highly inclined and laminated optical sheet microscopy we demonstrated that ARF4 enhanced NIS vesicular trafficking from the Golgi to the plasma membrane, whereas VCP - a principal component of ER-associated degradation - governed NIS proteolysis. Gene expression analysis indicated VCP expression was particularly induced in aggressive thyroid cancers and in patients who had poorer outcomes following RAI treatment. Two re-purposed Food and Drug Administration (FDA)-approved VCP inhibitors abrogated VCP-mediated repression of NIS function resulting in significantly increased NIS at the cell surface and markedly increased RAI uptake in mouse and human thyroid models. Collectively, these discoveries delineate NIS trafficking and highlight the new possibility of systemically enhancing RAI therapy in patients using FDA-approved drugs.

STATEMENT OF SIGNIFICANCE

Findings show that ARF4 and VCP are involved in NIS trafficking to the plasma membrane and highlight the possible therapeutic role of VCP inhibitors in enhancing radioiodine effectiveness in radioiodine-refractory thyroid cancer.

INTRODUCTION

Since the 1940s, radioiodine (RAI) treatment has been the central post-surgical therapy for patients with differentiated thyroid cancer (DTC) and ablative treatment with RAI is recommended in moderate and high-risk tumors (1). However, at least a quarter of patients with DTC do not uptake sufficient RAI for effective ablation (2, 3), which remains an urgent problem in metastatic disease. There are two cohorts of thyroid cancer patients: those who respond to RAI and have an excellent prognosis (radiosensitive tumors), and those who do not respond (radioresistant tumors) and whose outcome is dire (1). Despite efforts to improve outcomes, no substantial changes have been made to the way RAI is administered therapeutically. Troublingly, DTC is now the most rapidly increasing cancer in the UK and US, with 300,000 new cases reported worldwide per annum, and more than 40,000 deaths annually (4).

The sodium iodide symporter (NIS) is the sole human transporter responsible for iodide uptake (5), exploitation of which represents the first – and most specifically targeted – internal radiation therapy in existence. High-energy β-emitting ^{131}I is utilized to destroy remaining thyroid cells post-surgery, and target metastases. More recently, the interest in NIS has been enhanced due to its use as a novel reporter gene in preclinical and translational imaging systems and in theranostic strategies in non-thyroidal tumors (6, 7). Breast tumors, for instance, can uptake RAI (8), with functional NIS expression confirmed in up to ~80% of breast cancers (9). However, NIS is rarely localized to the plasma membrane (PM) in breast cancers, limiting its clinical utility (9, 10).

Decreased levels of NIS expression and/or diminished targeting of NIS to the PM represent the principal mechanisms behind radioiodine-refractory thyroid cancer (RAIR-TC) (11). Numerous studies have addressed the common pathways of NIS regulation *in vitro* and *in vivo* (12-14), such as key transcriptional and epigenetic alterations which silence thyroid-specific genes including NIS (15, 16). Clinical approaches to improve treatment of thyroid cancer have involved the use of retinoids (17), PPARγ agonists (18), MAPK pathway/BRAF inhibitors (19, 20), multi-targeted kinase inhibitors (21) and histone deacetylase (HDAC) inhibitors (22). Multiple biologically-targeted drugs have been evaluated in phase I, II and III trials, with several agents including sorafenib (21), lenvatinib (23) and dabrafenib (24) showing promising responses and/or disease stabilization. However, issues of toxicity and drug resistance remain.

To actively transport iodide for thyroid hormone biosynthesis and radioisotopes, NIS must be present at the basolateral PM. However, little is known about the mechanisms that govern

NIS trafficking. Thyroid-stimulating hormone (TSH) induces iodide uptake through upregulation of NIS expression and modulation of its subcellular localization (25). Yet, many thyroid cancers demonstrate reduced NIS activity through diminished PM retention (26, 27). BRAF-mutant tumors (60-70% of thyroid cancers) are more likely to be resistant to RAI, partly due to decreased NIS expression (12), but also impaired PM targeting (13, 28), through mechanisms which remain ill-defined. Currently, PTTG1-binding factor (PBF) is the only protein shown to bind NIS and modulate its subcellular localization (29).

Here, we performed mass spectrometry (MS/MS) to identify previously undefined proteins that interact with NIS and regulate its trafficking or retention at the PM. We now report two proteins – ADP-ribosylation factor 4 (ARF4) and valosin-containing protein (VCP) – which specifically bind NIS and directly regulate its function in both breast and thyroid cancer models. Critically, the ability to inhibit VCP activity via Food and Drug Administration (FDA)-approved drugs indicates a therapeutic possibility of systemically enhancing RAI uptake in patients. This provides new hope that NIS activity may be stimulated in RAIR-TC patients, but also supports the prospect of exploiting NIS trafficking and function to facilitate radioisotope uptake for *in vivo* imaging and therapy in non-thyroidal tumors.

MATERIALS AND METHODS

Cell culture and lentiviral cell line generation

Breast (MDA-MB-231) and thyroid (8505C, BCPAP, SW1736, TPC-1, CAL62) cancer cell lines were maintained in RPMI-1640 (Life Technologies), while HeLa cervical cancer cells were maintained in DMEM (Sigma-Aldrich). Media was supplemented with 10% fetal bovine serum (FBS), penicillin (10^5 U/l), and streptomycin (100 mg/l) and cell lines were maintained at 37^{o}C and 5% CO_2 in a humidified environment. Cell lines were obtained from ECACC (HeLa, MDA-MB-231) and DSMZ (8505C, BCPAP), while SW1736 and TPC-1 cell lines were kindly provided by Dr Rebecca Schweppe (University of Colorado). Cells were cultured at low passage, authenticated by short tandem repeat analysis (NorthGene) and tested for mycoplasma contamination (EZ-PCR kit; Geneflow).

Stable NIS-expressing MDA-MB-231 and TPC-1 cell lines were generated by lentiviral transduction, as per manufacturer's instructions. In brief, ready-to-transduce lentiviral particles containing a precision lentiORF construct (pLOC) housing cDNA coding for red fluorescent protein (*RFP)* (OHS5833) or the full-length human *NIS* cDNA without a stop codon within the open reading frame (ORF) (OHS5900-224632369) were purchased from Dharmacon. For lentiviral transduction the manufacturer's protocol was followed. In brief, one day after plating, MDA-MB-231 and TPC-1 cells were infected with the lentiviral vector containing *NIS* diluted in antibiotic-free and serum-free RPMI containing 8 μg/ml or 14 μg/ml polybrene respectively. Cells transduced with the *RFP*-containing lentiviral vector served as the control. After 24 hours, medium was replaced with RPMI containing 10% fetal bovine serum (FBS). After a further 48 hours, cells were maintained in RPMI containing 10% fetal bovine serum (FBS), penicillin (10^5 U/l), and streptomycin (100 mg/l) as well as 15 or 5 μg/ml *Blasticidin S* for the MDA-MB-231 and TPC-1 cell lines respectively. 24 hours later, infection efficiency was assessed by fluorescence microscopy. Upon cell expansion and selection of single cell colonies, NIS expression was assessed by quantitative PCR (qPCR) and Western blotting, with NIS function confirmed via the radioiodine uptake assay.

Mass spectrometry

NIS-interactors were isolated by co-immunoprecipitation (co-IP) (anti-NIS antibody) and separated by SDS-PAGE. Proteins were reduced, alkylated and trypsinised. Resulting peptides were separated on an acetonitrile gradient on the UltiMate 3000 HPLC (ThermoFisher Scientific). Eluted peptides passed through the AmaZon ETD ion trap and

tandem mass spectrometer (Bruker). Mass spectra were processed using the Bruker DataAnalysis software and analyzed using the Mascot search engine (Matrix Science). Datasets were filtered based on peptide number, DAVID functional classification (30, 31) and literature review (32-36) (Supplementary Table S1).

Nucleic acids and transfection

Plasmids containing human NIS cDNA with a HA- or MYC-tag have been described (37) and GFP-tagged NIS was kindly provided by Dr Takahiko Kogai (Dokkyo Medical University). NIS mutants $_{475}$ALAS$_{478}$ and $_{574}$AAAK$_{577}$ were generated using the QuikChange Site-directed Mutagenesis Kit (Agilent Technologies). Untagged-ARF4 plasmid was purchased from Origene (#SC119092) while wild type (WT) and mutant (QQ) VCP (rat) plasmid were kindly provided by Dr Yihong Ye (National Institutes of Health) (11, 12). Human VCP cDNA was generated by site-directed mutagenesis. Further details on nucleic acids and siRNA are provided (Supplementary Table S2 and S3). Plasmid DNA and siRNA transfections were performed with TransIT-LT1 (Mirus Bio) and Lipofectamine RNAiMAX (ThermoFisher Scientific) following standard protocols in accordance with the manufacturer's guidelines.

VCP inhibitors and Dynasore

All drugs were re-suspended in dimethyl sulfoxide (DMSO), diluted in RPMI then added directly to cells at the appropriate final concentration. Cells were treated with VCP inhibitors: Eeyarestatin-1 (ES-1) (Cayman Chemicals), NMS-873 (SelleckChem), Astemizole (Sigma-Aldrich), Clotrimazole (Sigma-Aldrich) and Ebastine (Sigma-Aldrich) or the dynamin inhibitor; Dynasore (Sigma-Aldrich).

Western blotting, cell-surface biotinylation, co-IP assays and RAI uptake

Western blotting, co-immunoprecipitation, cell surface biotinylation assays and RAI (^{125}I) uptake assays were performed as described (29, 38) following Dynasore treatment (2 hours), VCP inhibitor treatment (24 hours), DNA plasmid transfection (48 hours) or siRNA transfection (72 hours) as indicated.

Blots were probed with specific antibodies (Supplementary Table S4) and NIS expression quantified by densitometry in ImageJ relative to β-actin or Na^+/K^+ ATPase, as indicated.

Highly inclined and laminated optical sheet microscopy and proximity ligation assay

Live cell highly inclined and laminated optical sheet (HILO) microscopy was performed on an Olympus IX81 inverted fluorescence microscope. Images were acquired every 2 seconds for up to 5 minutes then integrated at 5 frames/second using the Olympus xCellence build 3554 software (Supplementary Movies S1 to 3). Mean velocity and distance travelled of NIS-GFP was quantified using the TrackMate plugin (ImageJ). The Duolink® *in situ* proximity ligation assay (PLA) was performed according to manufacturer's instructions (Sigma-Aldrich).

Gene expression data analyses

Normalized gene expression data and clinical information (Supplementary Table S5 to S7) for papillary thyroid cancer (PTC) and breast cancer were downloaded from TCGA via cBioPortal (39, 40) and FireBrowse (41). In total, RNA-seq data for 501 papillary thyroid cancer (THCA) and 1093 breast cancer (BRCA) TCGA samples were analyzed. Patient-derived poorly-differentiated thyroid cancer (PDTC) and anaplastic thyroid cancer (ATC) samples were selected from the Memorial Sloan Kettering Cancer Center pathology department files from 1986 – 2015 according to the classification outlined in (42). In total, mRNA expression data from fresh-frozen tissue was obtained from 17 PDTC and 20 ATC samples via MSK-IMPACT targeted sequencing. All 37 tumor samples were also expression profiled via the Affymetrix U133 plus 2.0 array and Agilent SurePrint G3 CGH 1x1M arrayCGH platform to validate copy number calls.

Statistical analyses

Data were analyzed using GraphPad Prism and Microsoft Excel (Supplementary Materials and Methods).

RESULTS

Identification and manipulation of NIS interactors

We performed MS/MS in MDA-MB-231 cells with lentivirally-expressed NIS (NIS+ve) to identify interactors in whole cell and PM extracts. NIS and its protein interactors were subjected to in-gel tryptic digest and resulting peptides were fingerprinted using the AmaZon ETD ion trap and tandem mass spectrometer prior to shortlisting (Fig. 1A and B; Supplementary Fig. S1A and B). Five proteins with established roles related to subcellular trafficking, endocytosis, PM targeting and/or endosomal transport were selected (Supplementary Fig. S1A and B; Supplementary Table S1) and underwent an initial endoribonuclease-prepared siRNA (esiRNA) screen to investigate their impact upon NIS function (Fig. 1C and D). An important finding was that ARF4 depletion repressed iodine-125 (RAI; ^{125}I) uptake in MDA-MB-231 NIS+ve cells, whereas VCP ablation resulted in a significant induction of RAI uptake (Fig. 1D). As a positive control, esiRNA knockdown of PBF, the only protein known to specifically modulate NIS subcellular localization and function (29), significantly increased ^{125}I uptake (Fig. 1C and D). In thyroidal TPC-1 NIS+ve cells, treatment with ARF4, VCP or PBF esiRNA also significantly altered RAI uptake (Supplementary Fig. S2A).

ARF4 and VCP were thus considered novel putative functional partners of NIS and further investigated. Subsequent ARF4 ablation in TPC-1 and MDA-MB-231 NIS+ve cells, as well as in human primary thyroid cells, confirmed a ~60-80% decrease in ^{125}I uptake (Fig. 1E) with different siRNA sequences (Supplementary Table S2). In contrast, transient ARF4 overexpression resulted in significantly increased ^{125}I uptake in all three cellular settings (Fig. 1F; Supplementary Fig. S2B), suggesting its impact on NIS function is bi-directional. A ~50-80% increase in ^{125}I uptake was further validated in VCP-siRNA-depleted TPC-1 and MDA-MB-231 NIS+ve cells, with human primary thyrocytes demonstrating a ~35% increase (Fig. 1G; Supplementary Table S2). VCP induction by transient transfection reversed these effects, resulting in markedly repressed ^{125}I uptake in all three cell models (Fig. 1H; Supplementary Fig. S2C).

Thus, we identify two novel modulators of NIS function which alter RAI uptake both in thyroid and breast cells lentivirally-transduced with NIS, and in human primary thyrocytes with endogenous NIS expression.

ARF4 and VCP bind NIS *in vitro* and modulate its expression

Having identified that manipulation of ARF4 and VCP expression altered RAI uptake, we sought to challenge our MS/MS data which indicated specific binding between each protein and NIS. Co-IP confirmed that NIS specifically interacts with ARF4 and VCP in both MDA-MB-231 and TPC-1 NIS+ve cells (Fig. 2A and B). Control co-IPs further demonstrated specific interaction between NIS with ARF4 and VCP (Supplementary Fig. S3A to D). Additionally, PLA demonstrated specific binding between ARF4 and NIS in three different cell types, which appeared to occur generally throughout the cytoplasm with some binding within the ER/Golgi also suggested (Fig. 2C; Supplementary Fig. S3E and F). Similarly, PLA confirmed the VCP: NIS interaction, which occurred more generally within the cytoplasm of MDA-MB-231, TPC-1 and HeLa cells (Fig. 2C; Supplementary Fig. S3E and F).

We next performed cell surface biotinylation assays to quantify whether ARF4 and VCP modulate the amount of NIS present at the PM. Exogenous expression of ARF4 in NIS+ve cells demonstrated an approximate doubling of NIS protein in PM preparations compared to vector only (VO) controls (Fig. 2D and E). In contrast, VCP overexpression resulted in significantly diminished NIS protein PM abundance (Fig. 2F and G). Together, these data suggest that whilst ARF4 potentiates NIS presence at the PM, VCP inhibits its expression at its key site of symporter activity.

ARF4 modulates NIS trafficking at the PM

Given that ARF4 and VCP overexpression were both associated with altered NIS PM localization, we next investigated their trafficking using highly inclined and laminated optical sheet (HILO) microscopy – a technique used to visualize and quantify molecular dynamics in cells. We identified ARF4-dsRED and NIS-GFP trafficking in co-incident vesicles at the PM in HeLa cells (Fig. 3A and B; Supplementary Fig. S4 A and B; Movie S1). By contrast, no such co-trafficking was apparent for VCP-dsRED and NIS-GFP, suggesting the site of functional interaction between VCP and NIS was distant to the PM (Supplementary Fig. S4C; Movie S2). Of particular significance, and in contrast to VCP, the presence of ARF4 led to an overall induction in both the mean velocity and distance travelled by NIS-GFP positive vesicles ($P < 0.001$; Fig. 3C and D; Supplementary Fig. S5A to C).

In control experiments, we confirmed that NIS is endosomally trafficked in association with clathrin (Supplementary Fig. S5D; Movie S3) and found a significant increase in the overall distance travelled by NIS-GFP in cells overexpressing clathrin (Supplementary Fig. S5A). We then appraised the impact of inhibiting clathrin-mediated endocytosis on NIS

function using 100 μM Dynasore; a cell-permeable inhibitor of dynamin, which is required for the budding and formation of clathrin-coated vesicles. Treatment of NIS+ve cells overexpressing ARF4 with Dynasore resulted in significantly greater RAI uptake (Fig. 3E) without any effect on total NIS protein levels (Fig. 3F; Supplementary Fig. S5E), suggesting ARF4 is not primarily enhancing NIS recycling to the PM.

ARF4 binds NIS via a C-terminal VXPX motif

ARF4 binds to the terminal VXPX motif of Rhodopsin (43). We identified two putative VXPX motifs within the extracellular loop of NIS at positions 475-478 (sequence VLPS) and the C-terminus at positions 574-577 (sequence VAPK). Abrogation of both motifs (mutations $_{475}$ALAS$_{478}$ and $_{574}$AAAK$_{577}$) resulted in NIS proteins which retained endogenous functionality, but the $_{574}$AAAK$_{577}$ NIS mutant could no longer be augmented in terms of RAI uptake by ARF4 overexpression in TPC-1 thyroid cells (Fig. 3G). Co-IP assays demonstrated that $_{475}$ALAS$_{478}$ mutant NIS still avidly bound ARF4, whereas $_{574}$AAAK$_{577}$ mutant NIS lost interaction (Fig. 3H). Hence, NIS has a C-terminal VXPX ARF4 recognition sequence which is required for ARF4 potentiation of function.

Overall, our results indicate that ARF4 and VCP appear to have different modes of action; ARF4 is implicated in the trafficking of NIS to the PM, whereas VCP binds NIS and modulates NIS function elsewhere in the cell. In support of this, significantly altered total NIS protein levels were apparent in NIS+ve cells after siRNA ablation or exogenous expression of VCP but not following modulation of ARF4 expression (Supplementary Fig. S6A and B).

Selective VCP inhibitors promote RAI uptake

VCP functions chiefly as a chaperone in disassembling protein complexes and facilitating the extraction and/or proteasomal degradation of proteins from the endoplasmic reticulum (ER), but is also implicated in a wider range of other cellular actions (44). Several specific VCP inhibitors already exist which target different facets of VCP structure/activity (45). Critically, a significant induction of RAI uptake (Fig. 4A) was evident in NIS+ve cells treated with the allosteric VCP inhibitor Eeyarestatin-1 (ES-1), which inhibits ER-cytosol dislocation and subsequent degradation of substrates (46). Similarly, the VCP inhibitor NMS-873, which is a potent and specific allosteric inhibitor of VCP (47), yielded a significant 3-4-fold increase in RAI uptake in NIS+ve cells (Fig. 4B).

Importantly, there were no significant reductions in cell viability at the optimal doses of VCP inhibitors used (Supplementary Fig. S6C), nor any changes in VCP protein expression (Fig. 4C). PLA and co-IP assays also revealed that NIS and VCP retained the ability to bind in the presence of VCP inhibitors (Fig. 4D and E). Notably, we also observed a significant induction in RAI uptake after 24 hours of ES-1 and NMS-873 inhibitor treatment on native thyroidal cells (i.e. without lentiviral NIS) with different mutation profiles, including TPC-1 (Fig. 4F and G), CAL-62, 8505C, BCPAP and SW1736 cells (Supplementary Fig. S6D to G). This important finding raises the possibility that VCP inhibitors can be used to induce RAI uptake in thyroid cells that have inherently repressed NIS function.

Dissecting the VCP mechanism of action

We next examined the dynamics of therapeutically targeting VCP and found that ES-1 was associated with increased detectable NIS protein after 12 hours, accompanied by a concomitant increase in RAI uptake by 24 hours (Fig. 4H). Similar data were apparent for NMS-873, although RAI uptake and NIS expression were detected at 6 hours post-treatment (Fig. 4I). To explore the dependency of ES-1 on the presence of VCP to modulate RAI uptake, we characterized VCP-ablated TPC-1 NIS+ve cells which demonstrated no induction of RAI uptake after ES-1 (Fig. 4J) or NMS-873 treatment (Supplementary Fig. S7A). Thus, confirming that inhibitors ES-1 and NMS-873 require VCP in order to exert their effects on NIS function.

VCP's canonical function lies in facilitating the extraction of misfolded proteins from the ER, a 'segregase' process which generally requires ATPase activity. We next used an ATPase-deficient dominant-negative VCP mutant (QQ VCP) to investigate whether VCP required ATPase activity to modulate NIS function. The QQ VCP mutant behaved identically to wild type VCP (WT VCP) in repressing RAI uptake when overexpressed in multiple cell models (Fig. 4K) and retained the ability to decrease NIS localization at the PM in cell surface biotinylation assays (Supplementary Fig. S7B). Additionally, ATP-competitive VCP inhibitors N2,N4-dibenzylquinazoline-2,4-diamine (DBeQ) (48) and sorafenib, which inhibits VCP activity at the PM by blocking its phosphorylation, failed to increase RAI uptake in NIS+ve cells (Supplementary Fig. S7C and D). Collectively, these results suggest that VCP functions in an ATPase-independent manner to affect NIS function, a facet which has been reported in VCP's ability to unfold proteins for subsequent proteasomal degradation (49).

Recently, three new drugs – astemizole, clotrimazole and ebastine – have been identified as re-purposed small molecules which specifically and allosterically inhibit VCP activity

(50). Clotrimazole and ebastine are well tolerated *in vivo* and FDA-approved (50). As ES-1 and NMS-873 may have limited clinical utility (51), we investigated whether astemizole, clotrimazole and ebastine also enhance RAI uptake. All three drugs significantly induced RAI uptake (Fig. 5A) without affecting cell viability (Supplementary Fig. S6C). There was no induction of RAI uptake after treatment of VCP-ablated TPC-1 NIS+ve cells, thus confirming these VCP inhibitors require VCP in order to exert their effect on NIS function (Fig. 5B and C). Additionally, VCP inhibitors increased NIS expression, particularly at the PM (Fig. 5D and E) but did not alter VCP protein levels (Fig. 5F).

We next progressed to our model of mouse thyroid function. Primary thyrocytes were isolated from C57BL/6 mice and treated with ebastine or clotrimazole; both drugs significantly enhanced RAI uptake and NIS protein expression (Fig. 5G to I). Finally, we tested our drugs in human primary thyroid cultures, which were confirmed TSH-responsive. Here, both ebastine and clotrimazole significantly increased RAI uptake (Fig. 5J).

VCP and ARF4 expression correlates with poorer survival and response to RAI

Having identified VCP and ARF4 as novel regulators of NIS function, we appraised their expression profiles and clinical relevance in thyroid cancer using The Cancer Genome Atlas (TCGA) papillary thyroid cancer (THCA) dataset. Of significance, ARF4 was under-expressed in PTC compared to normal tissue (Fig. 6A), while VCP was significantly induced in PTC, PDTC and ATC (Fig. 6A and B). Genetic drivers in PTC have distinct signaling consequences and have been categorized into BRAF-like and RAS-like PTCs according to distinct gene signatures (52). Interestingly, VCP mRNA expression did not differ between BRAF-like and RAS-like PTC, while ARF4 mRNA expression was lower in BRAF-like than RAS-like tumors across the THCA series (Fig. 6C).

In agreement with these findings, there was greater reduction of ARF4 expression in BRAF-mutant PTC versus the non-BRAF mutant tumors (Fig. 6D). The frequency of *BRAF* alterations was also higher in PTC with low ARF4 expression compared to PTC with high ARF4 (Fig. 6E). By comparison, VCP expression was most significantly elevated in PTC with *BRAF* mutant, *RET* fusion and *PAX8* fusion genes (Fig. 6F). In contrast to ARF4, there was a similar frequency of *BRAF* alterations in PTC with either high or low VCP expression (Fig. 6G).

We next evaluated whether VCP and ARF4 expression were associated with patient outcome, treatment (RAI versus non-RAI) or disease classification. Overall, log-rank analysis using the entire cohort (n=413) did not detect any difference in survival between PTC

patients with high tumoral VCP compared to those with low VCP (P_L=NS), although a significant difference was evident at early (P_B=0.016) and intermediate time-points (P_T=0.022; Fig. 6H). Similarly, to THCA, higher VCP expression was present in breast tumors versus normal tissue in the BRCA cohort (Supplementary Fig. S8A), which again failed to correlate with a significant reduction in survival (P_L=NS; Supplementary Fig. S8B).

A key finding however was that the subgroup of RAI-treated PTC patients with high tumoral VCP expression (n=195) had significantly reduced disease-free survival (DFS) than those with low VCP (P_L=0.016; Fig. 6I; Supplementary Fig. S8C). By comparison, there was no significant difference in DFS of patients that did not receive RAI treatment when stratified on median tumoral VCP (Fig. 6J). Cox regression analysis further highlighted that higher tumoral VCP in RAI-treated PTC patients was associated with an increased risk of recurrence (Hazard ratio (HR) 3.57; Fig. 6K). Interestingly, the risk of recurrence was even greater for RAI-treated patient subgroups associated with BRAF-like (HR 4.63) or BRAF alterations (HR 4.97; Fig. 6K; Supplementary Fig. S8D to G). RAI-treated patients with lower tumoral ARF4 expression receiving a dose ≥100mCi also had reduced survival (Fig. 6L and M and Supplementary Fig. S8H and I) and a higher risk of recurrence (HR 2.93; Fig. 6K). In contrast, there was no increase in the risk of recurrence of non-RAI treated PTC patients with higher tumoral VCP or lower ARF4 expression (Fig. 6K). Overall, disease classification indicated that RAI-treated patients had significantly more advanced thyroid disease than non-RAI treated patients (Supplementary Fig. S9A; Supplementary Table S5). Importantly, there were no significant differences in clinical staging attributes for RAI or non-RAI treatment groups stratified for VCP or ARF4 tumoral expression (Supplementary Fig. S9B and C; Supplementary Table S6 and 7).

Collectively, we show that ARF4 and VCP are significantly dysregulated in PTC, with expression profiles which fit the repression of RAI uptake generally apparent in thyroid cancers. We propose that dysregulated ARF4 and VCP results in reduced trafficking of NIS to the PM via repressed ARF4 function and increased VCP activity in targeting NIS for degradation. We further identify that VCP and ARF4 are associated with poorer survival characteristics in RAI-treated patients and represent promising new drug targets in patients who are RAI-refractory. A model of the proposed functional interaction of NIS with VCP and ARF4 is outlined in Fig. 7.

DISCUSSION

Extensive studies have sought to enhance NIS expression and function in patients with RAIR-TC, and hence re-sensitize tumors to RAI therapy. This is essential because patients with RAIR-TC, particularly those with metastatic disease, have a life expectancy of 3–5 years and represent a group for whom there is a clear unmet medical need (2, 3). Most investigations so far have focused on 're-differentiation agents', which stimulate the expression of thyroid-specific genes including NIS. Constitutive activation of the MAPK pathway in thyroid cancer results in dysregulated NIS expression and function, decreased RAI uptake and a poor patient prognosis. A substantial number of studies have therefore focused on selective inhibitors of the MAPK pathway to restore RAI avidity (20, 53).

Importantly, new drug strategies, such as combining BRAF or MEK inhibitors with pan-PI3K inhibitors, are showing pre-clinical promise by rescuing NIS gene expression in thyroid cancer (19). However, we propose that augmenting NIS trafficking to the PM is fundamental to boosting the efficacy of radioisotope treatment, given that we are now close to having the necessary tools to restore NIS expression. With the advent of NIS-based *in vivo* imaging and therapeutic approaches in non-thyroidal malignancies and other disease modalities, the exploitation and enhancement of NIS function via FDA-approved VCP inhibitors has widespread clinical potential. For example, NIS expression can now be induced via administration of engineered viruses or mesenchymal stem cells in tumoral and non-tumoral settings, including cardiac disease and tissue regeneration (6, 54, 55)

Here, we have identified five allosteric inhibitors of VCP which all enhanced RAI uptake *in vitro* by a minimum of two-fold. Specific ARF4 agonists do not currently exist, and hence we pursued VCP inhibition as our central therapeutic strategy. To circumvent potential issues of toxicity we evaluated alternative drugs to enhance RAI uptake, of which ebastine and clotrimazole are FDA-approved and well tolerated *in vivo* (50). Given that RAI uptake was enhanced within 24 hours of ebastine or clotrimazole treatment, our findings necessitate the need for clinical trials to address whether patients receiving these drugs at the time of RAI therapy uptake more ^{131}I. One important finding in support of this is that native, relatively de-differentiated thyroid cells which have negligible endogenous RAI uptake in our hands showed measurable NIS function following VCP inhibition.

Previously PBF which, unlike NIS, has a functional endocytosis motif (38), was the only protein shown to bind NIS and diminish its function due to altered subcellular localization via endocytosis (29). Now, our MS/MS, co-IP and PLA assays have identified and validated ARF4 and VCP as novel NIS interactors. ARF4 binds NIS via a C-terminal $_{574}$VXPX$_{577}$ motif

to traffic NIS towards the PM and enhance NIS function. One surprising facet observed via new imaging technologies was the rapid movement of vesicles expressing ARF4 and NIS, which hint at a more dynamic process of NIS trafficking than previously suggested. ARF4 has a range of subcellular roles, from recruiting adaptor proteins for packaging proteins into vesicles destined for the PM, to recycling proteins from the PM through endosomes (56). Our data suggest ARF4 is involved in the vesicular transport of NIS to the PM, given that inhibition of endocytosis had no impact on the ARF4-mediated increase in RAI uptake.

An important clinical observation was that high tumoral VCP expression, which acts predominately in the ER, and hence early in the progression of NIS to the PM, was strongly correlated with DFS, both overall, but particularly in patients who received RAI treatment. Similarly, PTC patients with low tumoral ARF4 expression who received higher doses of RAI (≥100 mCi) also had a significantly worse DFS. In accordance with ATA guidelines (1), RAI-treated patients in TCGA had more advanced disease than non-RAI treated patients. However, there was no significant difference in clinical staging attributes for RAI or non-RAI treatment groups stratified for VCP or ARF4 tumoral expression. Importantly, these findings suggest that altered expression of VCP or ARF4 do not contribute to the advancement of thyroid disease. Instead we propose that high VCP or low ARF4 expression significantly influence outcomes following RAI treatment through modulating the function of NIS. Our hypothesis is that high tumoral VCP expression in patients with PTC results in increased NIS degradation, permitting less NIS to be trafficked to the PM by ARF4, which we show is repressed in PTC. Hence the function of NIS, which is already at very low expression levels or predominantly localized to intracellular compartments, in PTC, is further attenuated resulting in worse DFS. In agreement with this, VCP or ARF4 expression did not significantly influence disease recurrence in patients that had not received RAI treatment.

Several gaps in our knowledge remain. As a protein expressed mainly in basolateral membranes, cell polarization is important to NIS function. No human polarized cell models are physiologically relevant to thyroid cell biology, however. Despite this, our studies in non-polarized cell systems demonstrate a universal mechanism of NIS trafficking in transformed thyroid and breast cells, as well as primary human and mouse thyrocytes. Further, since our de-differentiated TPC-1 thyroid cells, as well as our MDA-MB-231 breast cells, are unlikely to express physiologically relevant levels of the TSH receptor, we did not investigate the potential effects of the canonical regulator of NIS – TSH – on NIS trafficking (57). Our hypothesis is that TSH is more important to the expression of NIS than its subcellular trafficking. This reflects the surprising timescales of trafficking we observed in our HILO

microscopy; whereby TSH is known to influence NIS function over the course of hours and days (57), in contrast to the vesicular movement of NIS close to the PM, which was unexpectedly dynamic. We thus propose that NIS function at the PM is considerably more rapid than currently envisaged.

Collectively, we now identify two novel NIS interactors, VCP and ARF4, with critical roles in modulating NIS function as well as correlating markedly with clinical outcome in PTC. Notably, VCP is specifically-druggable with FDA-approved inhibitors resulting in enhanced RAI uptake in breast and thyroid cancer models. Strategies that manipulate the function/expression of VCP or ARF4 will thus offer a promising new therapeutic strategy for RAIR-TC in addition to augmenting NIS function for novel *in vivo* imaging and therapeutic strategies across a broad disease spectrum.

ACKNOWLEDGEMENTS

This work was supported by the Medical Research Council (MR/P000509/1 to C.J. McCabe, V.E. Smith, and K. Boelaert) and Wellcome Trust (RG_05-052 to A. Fletcher). C.J. McCabe also received funding from Cancer Research UK, Get A-Head Charitable Trust, and a PhD studentship from the Medical Research Council/University of Birmingham. We acknowledge the contribution to this study by the Human Biomaterials Resource Centre (University of Birmingham), A. Di Maio and D. Calebiro for expertise in HILO, and D. Nasteska and D. Hodson for C57BL/6 mice.

REFERENCES

1. Haugen BR, Alexander EK, Bible KC, Doherty GM, Mandel SJ, Nikiforov YE, et al. 2015 American Thyroid Association Management Guidelines for Adult Patients with Thyroid Nodules and Differentiated Thyroid Cancer: The American Thyroid Association Guidelines Task Force on Thyroid Nodules and Differentiated Thyroid Cancer. Thyroid. 2016;26:1-133.
2. Schlumberger M, Brose M, Elisei R, Leboulleux S, Luster M, Pitoia F, et al. Definition and management of radioactive iodine-refractory differentiated thyroid cancer. Lancet Diabetes Endocrinol. 2014;2:356-8.
3. Spitzweg C, Bible KC, Hofbauer LC, Morris JC. Advanced radioiodine-refractory differentiated thyroid cancer: the sodium iodide symporter and other emerging therapeutic targets. Lancet Diabetes Endocrinol. 2014;10:830-42.
4. La Vecchia C, Malvezzi M, Bosetti C, Garavello W, Bertuccio P, Levi F, et al. Thyroid cancer mortality and incidence: a global overview. Int J Cancer. 2015;136:2187-95.
5. Dai G, Levy O, Carrasco N. Cloning and characterization of the thyroid iodide transporter. Nature. 1996;379:458-60.
6. Ravera S, Reyna-Neyra A, Ferrandino G, Amzel LM, Carrasco N. The Sodium/Iodide Symporter (NIS): Molecular Physiology and Preclinical and Clinical Applications. Annu Rev Physiol. 2017;79:261-89.
7. Urnauer S, Schmohl KA, Tutter M, Schug C, Schwenk N, Morys S, et al. Dual-targeted NIS polyplexes-a theranostic strategy toward tumors with heterogeneous receptor expression. Gene Ther. 2019;26:93-108.
8. Eskin BA, Parker JA, Bassett JG, George DL. Human breast uptake of radioactive iodine. Obstet Gynecol. 1974;44:398-402.
9. Tazebay UH, Wapnir IL, Levy O, Dohan O, Zuckier LS, Zhao QH, et al. The mammary gland iodide transporter is expressed during lactation and in breast cancer. Nat Med. 2000;6:871-8.
10. Moon DH, Lee SJ, Park KY, Park KK, Ahn SH, Pai MS, et al. Correlation between 99mTc-pertechnetate uptakes and expressions of human sodium iodide symporter gene in breast tumor tissues. Nucl Med Biol. 2001;28:829-34.
11. Spitzweg C, Harrington KJ, Pinke LA, Vile RG, Morris JC. Clinical review 132: The sodium iodide symporter and its potential role in cancer therapy. J Clin Endocrinol Metab. 2001;86:3327-35.
12. Riesco-Eizaguirre G, Gutierrez-Martinez P, Garcia-Cabezas MA, Nistal M, Santisteban P. The oncogene BRAF V600E is associated with a high risk of recurrence and less differentiated papillary thyroid carcinoma due to the impairment of Na+/I- targeting to the membrane. Endocr Relat Cancer. 2006;13:257-69.
13. Riesco-Eizaguirre G, Rodriguez I, De la Vieja A, Costamagna E, Carrasco N, Nistal M, et al. The BRAFV600E oncogene induces transforming growth factor beta secretion leading to sodium iodide symporter repression and increased malignancy in thyroid cancer. Cancer Res. 2009;69:8317-25.
14. Kogai T, Sajid-Crockett S, Newmarch LS, Liu YY, Brent GA. Phosphoinositide-3-kinase inhibition induces sodium/iodide symporter expression in rat thyroid cells and human papillary thyroid cancer cells. J Endocrinol. 2008;199:243-52.
15. Mancikova V, Buj R, Castelblanco E, Inglada-Perez L, Diez A, de Cubas AA, et al. DNA methylation profiling of well-differentiated thyroid cancer uncovers markers of recurrence free survival. Int J Cancer. 2014;135:598-610.
16. Kitazono M, Robey R, Zhan Z, Sarlis NJ, Skarulis MC, Aikou T, et al. Low concentrations of the histone deacetylase inhibitor, depsipeptide (FR901228), increase expression of the Na(+)/I(-) symporter and iodine accumulation in poorly differentiated thyroid carcinoma cells. J Clin Endocrinol Metab. 2001;86:3430-5.

17. Kogai T, Kanamoto Y, Che LH, Taki K, Moatamed F, Schultz JJ, et al. Systemic retinoic acid treatment induces sodium/iodide symporter expression and radioiodide uptake in mouse breast cancer models. Cancer Res. 2004;64:415-22.
18. Kebebew E, Peng M, Reiff E, Treseler P, Woeber KA, Clark OH, et al. A phase II trial of rosiglitazone in patients with thyroglobulin-positive and radioiodine-negative differentiated thyroid cancer. Surgery. 2006;140:960-6.
19. Nagarajah J, Le M, Knauf JA, Ferrandino G, Montero-Conde C, Pillarsetty N, et al. Sustained ERK inhibition maximizes responses of BrafV600E thyroid cancers to radioiodine. J Clin Invest. 2016;126:4119-24.
20. Dunn LA, Sherman EJ, Baxi SS, Tchekmedyian V, Grewal RK, Larson SM, et al. Vemurafenib Redifferentiation of BRAF Mutant, RAI-Refractory Thyroid Cancers. J Clin Endocrinol Metab. 2019;104:1417-28.
21. Hoftijzer H, Heemstra KA, Morreau H, Stokkel MP, Corssmit EP, Gelderblom H, et al. Beneficial effects of sorafenib on tumor progression, but not on radioiodine uptake, in patients with differentiated thyroid carcinoma. Eur J Endocrinol. 2009;161:923-31.
22. Piekarz RL, Frye R, Turner M, Wright JJ, Allen SL, Kirschbaum MH, et al. Phase II multi-institutional trial of the histone deacetylase inhibitor romidepsin as monotherapy for patients with cutaneous T-cell lymphoma. J Clin Oncol. 2009;27:5410-7.
23. Schlumberger M, Tahara M, Wirth LJ, Robinson B, Brose MS, Elisei R, et al. Lenvatinib versus placebo in radioiodine-refractory thyroid cancer. N Engl J Med. 2015;372:621-30.
24. Rothenberg SM, McFadden DG, Palmer EL, Daniels GH, Wirth LJ. Redifferentiation of iodine-refractory BRAF V600E-mutant metastatic papillary thyroid cancer with dabrafenib. Clin Cancer Res. 2015;21:1028-35.
25. Kogai T, Curcio F, Hyman S, Cornford EM, Brent GA, Hershman JM. Induction of follicle formation in long-term cultured normal human thyroid cells treated with thyrotropin stimulates iodide uptake but not sodium/iodide symporter messenger RNA and protein expression. J Endocrinol. 2000;167:125-35.
26. Castro MR, Bergert ER, Beito TG, Roche PC, Ziesmer SC, Jhiang SM, et al. Monoclonal antibodies against the human sodium iodide symporter: utility for immunocytochemistry of thyroid cancer. J Endocrinol. 1999;163:495-504.
27. Dohan O, Baloch Z, Banrevi Z, Livolsi V, Carrasco N. Rapid communication: predominant intracellular overexpression of the Na(+)/I(-) symporter (NIS) in a large sampling of thyroid cancer cases. J Clin Endocrinol Metab. 2001;86:2697-700.
28. Riesco-Eizaguirre G, Santisteban P. A perspective view of sodium iodide symporter research and its clinical implications. EurJEndocrinol. 2006;155:495-512.
29. Smith VE, Read ML, Turnell AS, Watkins RJ, Watkinson JC, lewy gd, et al. A novel mechanism of sodium iodide symporter repression in differentiated thyroid cancer. J Cell Sci. 2009;122:3393-402.
30. Huang DW, Sherman BT, Tan Q, Collins JR, Alvord WG, Roayaei J, et al. The DAVID Gene Functional Classification Tool: a novel biological module-centric algorithm to functionally analyze large gene lists. Genome Biol. 2007;8:R183.
31. Huang DW, Sherman BT, Tan Q, Kir J, Liu D, Bryant D, et al. DAVID Bioinformatics Resources: expanded annotation database and novel algorithms to better extract biology from large gene lists. Nucleic Acids Res. 2007;35:W169-75.
32. Cotomacci G, Sarkis JJ, Furstenau CR, Barreto-Chaves ML. Thyroid hormones are involved in 5'-nucleotidase modulation in soluble fraction of cardiac tissue. Life Sci. 2012;91:137-42.
33. Li S, Esterberg R, Lachance V, Ren D, Radde-Gallwitz K, Chi F, et al. Rack1 is required for Vangl2 membrane localization and planar cell polarity signaling while attenuating canonical Wnt activity. Proc Natl Acad Sci U S A. 2011;108:2264-9.
34. Myklebust LM, Akslen LA, Varhaug JE, Lillehaug JR. Receptor for activated protein C kinase 1 (RACK1) is overexpressed in papillary thyroid carcinoma. Thyroid. 2011;21:1217-25.

35. Tamajusuku AS, Carrillo-Sepulveda MA, Braganhol E, Wink MR, Sarkis JJ, Barreto-Chaves ML, et al. Activity and expression of ecto-5'-nucleotidase/CD73 are increased by thyroid hormones in vascular smooth muscle cells. Mol Cell Biochem. 2006;289:65-72.
36. Yang J, Liao X, Yu J, Zhou P. Role of CD73 in Disease: Promising Prognostic Indicator and Therapeutic Target. Curr Med Chem. 2018;25:2260-71.
37. Ye Y, Meyer HH, Rapoport TA. The AAA ATPase Cdc48/p97 and its partners transport proteins from the ER into the cytosol. Nature. 2001;414:652-6.
38. Smith VE, Sharma N, Read ML, Ryan G, Martin A, Boelaert K, et al. Manipulation of PBF/PTTG1IP phosphorylation status; a new therapeutic strategy for improving radioiodine uptake in thyroid and other tumours. J Clin Endocrinol Metab 2013;98:2876-86.
39. Cerami E, Gao J, Dogrusoz U, Gross BE, Sumer SO, Aksoy BA, et al. The cBio cancer genomics portal: an open platform for exploring multidimensional cancer genomics data. Cancer Discov. 2012;2:401-4.
40. Gao J, Aksoy BA, Dogrusoz U, Dresdner G, Gross B, Sumer SO, et al. Integrative analysis of complex cancer genomics and clinical profiles using the cBioPortal. Sci Signal. 2013;6:pl1.
41. Broad Institute TCGA Genome Data Analysis Center: Analysis-ready standardized TCGA data from Broad GDAC Firehose 2016_01_28 run. Broad Institute of MIT and Harvard. Dataset 2016. DOI: 10.7908/C11G0KM9.
42. Landa I, Ibrahimpasic T, Boucai L, Sinha R, Knauf JA, Shah RH, et al. Genomic and transcriptomic hallmarks of poorly differentiated and anaplastic thyroid cancers. J Clin Invest. 2016;126:1052-66.
43. Deretic D, Williams AH, Ransom N, Morel V, Hargrave PA, Arendt A. Rhodopsin C terminus, the site of mutations causing retinal disease, regulates trafficking by binding to ADP-ribosylation factor 4 (ARF4). Proc Natl Acad Sci U S A. 2005;102:3301-6.
44. Bastola P, Neums L, Schoenen FJ, Chien J. VCP inhibitors induce endoplasmic reticulum stress, cause cell cycle arrest, trigger caspase-mediated cell death and synergistically kill ovarian cancer cells in combination with Salubrinal. Mol Oncol. 2016;10:1559-74.
45. Chapman E, Maksim N, de la Cruz F, La Clair JJ. Inhibitors of the AAA+ chaperone p97. Molecules. 2015;20:3027-49.
46. Wang Q, Li L, Ye Y. Inhibition of p97-dependent protein degradation by Eeyarestatin I. J Biol Chem. 2008;283:7445-54.
47. Magnaghi P, D'Alessio R, Valsasina B, Avanzi N, Rizzi S, Asa D, et al. Covalent and allosteric inhibitors of the ATPase VCP/p97 induce cancer cell death. Nat Chem Biol. 2013;9:548-56.
48. Chou TF, Brown SJ, Minond D, Nordin BE, Li K, Jones AC, et al. Reversible inhibitor of p97, DBeQ, impairs both ubiquitin-dependent and autophagic protein clearance pathways. Proc Natl Acad Sci U S A. 2011;108:4834-9.
49. Song C, Wang Q, Song C, Rogers TJ. Valosin-containing protein (VCP/p97) is capable of unfolding polyubiquitinated proteins through its ATPase domains. Biochem Biophys Res Commun. 2015;463:453-7.
50. Segura-Cabrera A, Tripathi R, Zhang X, Gui L, Chou TF, Komurov K. A structure- and chemical genomics-based approach for repositioning of drugs against VCP/p97 ATPase. Sci Rep. 2017;7:44912.
51. Bastola P, Oien DB, Cooley M, Chien J. Emerging Cancer Therapeutic Targets in Protein Homeostasis. AAPS J. 2018;20:94.
52. Cancer Genome Atlas Research N. Integrated genomic characterization of papillary thyroid carcinoma. Cell. 2014;159:676-90.
53. Zhang H, Chen D. Synergistic inhibition of MEK/ERK and BRAF V600E with PD98059 and PLX4032 induces sodium/iodide symporter (NIS) expression and radioiodine uptake in BRAF mutated papillary thyroid cancer cells. Thyroid Res. 2018;11:13.

54. Hickey RD, Mao SA, Amiot B, Suksanpaisan L, Miller A, Nace R, et al. Noninvasive 3-dimensional imaging of liver regeneration in a mouse model of hereditary tyrosinemia type 1 using the sodium iodide symporter gene. Liver Transpl. 2015;21:442-53.
55. Knoop K, Schwenk N, Schmohl K, Muller A, Zach C, Cyran C, et al. Mesenchymal stem cell-mediated, tumor stroma-targeted radioiodine therapy of metastatic colon cancer using the sodium iodide symporter as theranostic gene. J Nucl Med. 2015;56:600-6.
56. Wang J, Fresquez T, Kandachar V, Deretic D. The Arf GEF GBF1 and Arf4 synergize with the sensory receptor cargo, rhodopsin, to regulate ciliary membrane trafficking. J Cell Sci. 2017;130:3975-87.
57. Riedel C, Dohan O, De la Vieja A, Ginter CS, Carrasco N. Journey of the iodide transporter NIS: from its molecular identification to its clinical role in cancer. Trends Biochem Sci. 2001;26:490-6.

FIGURE LEGENDS

Figure 1. Identification of ARF4 and VCP as regulators of NIS activity. (*A*) Western blot analysis of whole cell lysate and PM fraction in MDA-MB-231 (NIS+ve) cells used in MS/MS. (*B*) Top hits for putative NIS interactors identified by MS/MS (peptides≥6). Highlighted proteins selected for further study. (*C-D*) Western blot analysis and RAI uptake of MDA-MB-231 (NIS+ve) cells transfected with esiRNA specific for indicated NIS interactors. NT – non-transfected cells. Western blot analysis and RAI uptake in MDA-MB-231 (NIS+ve) cells, TPC-1 (NIS+ve) cells and human primary thyrocytes transfected with ARF4 siRNA (*E*), or ARF4 (*F*). Same as (*E-F*) but cells transfected with VCP siRNA (*G*), or VCP (*H*). NS, not significant; *, $P<0.05$; ***, $P<0.001$.

Figure 2. ARF4 and VCP bind NIS *in vitro* and modulate PM NIS. (*A*) Co-IP assays in MDA-MB-231 (NIS+ve) cells showing specific interaction between NIS and ARF4 (left) or VCP (right). (*B*) Same as (*A*), but in TPC-1 (NIS+ve) cells. (*C*) PLA demonstrating specific interaction between NIS-MYC and ARF4 (upper) or VCP (lower) in MDA-MB-231, TPC-1 and HeLa cells. Red fluorescent spots indicate specific interactions. Blue indicates DAPI nuclear staining. Magnification, 100X. Scale bars, 10 μM. Western blot analysis of NIS protein levels at the PM relative to Na^+/K^+ ATPase following the CSBA in TPC-1 (NIS+ve) (*D*) and MDA-MB-231 (NIS+ve) cells (**E**) after ARF4 transfection. (*F-G*) Same as (*D-E*) but after VCP transfection. *, $P<0.05$; ***, $P<0.001$.

Figure 3. Involvement of ARF4 in trafficking NIS at the PM (*A-B*) HILO microscopy images demonstrating trafficking of ARF4-dsRED (red), NIS-GFP (green) and co-localization (yellow) to the PM in HeLa cells. Video capture times (hr:min:sec) are indicated. PM regions in framed areas are magnified in bottom-right panels which highlight the movement of ARF4 and NIS (white and orange arrowheads; see lower panels). Scale bars, 10 μM. (*C*) Representative images of NIS-GFP movement patterns tracked using ImageJ software. Scale bars, 10 μM. (*D*) Box-whisker plot of velocity (μm/sec) and distance travelled (μm) of NIS-GFP in HeLa cells transfected with ARF4 (n=475) or VO (n=339). (*E*) RAI uptake in TPC-1 (NIS+ve) and MDA-MB-231 (NIS+ve) cells transfected with ARF4 and treated with Dynasore for 1 hour prior to addition of ^{125}I. (*F*) Western blot analysis of NIS expression levels in TPC-1 (NIS+ve) cells as described in (*E*)**.** (*G*) RAI uptake in TPC-1 cells transfected with ARF4, as well as wildtype (WT) NIS, $_{574}AAAK_{577}$ mutant NIS or $_{475}ALAS_{478}$ mutant

NIS. (*H*) Representative co-IP assay for ARF4 with WT or mutant NIS. NS, not significant; *, $P<0.05$; ***, $P<0.001$.

Figure 4. Inhibition of VCP enhances NIS function. (*A*) RAI uptake of MDA-MB-231 (NIS+ve) and TPC-1 (NIS+ve) cells treated with ES-1 for 24 hours. (*B*) Same as (*A*) but cells treated with NMS-873. (*C*) Western blot analysis following ES-1 or NMS-873 treatment in TPC-1 (NIS+ve) cells. (*D*) PLA showing specific interaction (red fluorescent spots) between NIS-MYC and VCP in TPC-1 cells treated with ES-1. Blue indicates DAPI nuclear stain. Magnification, 100X. Scale bars, 10 μM. (*E*) Co-IP assays demonstrating interaction of VCP and NIS in TPC-1 (NIS+ve) cells treated with ES-1 or NMS-873. (*F-G*) RAI uptake and relative NIS protein levels in parental TPC-1 cells treated with ES-1, NMS-873 or DMSO. (*H*) Time-course of RAI uptake (upper) and relative NIS protein levels (lower) in TPC-1 (NIS+ve) cells treated with 2.5 μM ES-1. (*I*) Same as (*H*) but cells treated with 5 μM NMS-873. (*J*) RAI uptake and Western blot analysis in TPC-1 (NIS+ve) cells transfected with VCP or Scr siRNA, then treated with ES-1. (*K*) RAI uptake and Western blot analysis in MDA-MB-231 (NIS+ve) cells, TPC-1 (NIS+ve) cells and human primary thyrocytes transfected with WT VCP or QQ VCP mutant. NS, not significant; *, $P<0.05$; **, $P<0.01$; ***, $P<0.001$.

Figure 5. VCP inhibitors increase PM NIS expression and function. (A) TPC-1 (NIS+ve) cells treated with VCP inhibitors (Ebastine, Clotrimazole and Astemizole). Western blot (B) and RAI uptake (C) analyses of VCP expression following VCP-siRNA depletion and treatment with 0.5 μM Ebastine (upper), 0.25 μM Clotrimazole (middle), 0.25 μM Astemizole (lower) in TPC-1 (NIS+ve) cells. (D-E) Cell surface biotinylation assay analysis of NIS protein levels at the PM relative to Na+/K+ ATPase in the TPC-1 (NIS+ve) cell line after treatment with 0.5 μM Ebastine, 0.25 μM Clotrimazole or 0.25 μM Astemizole. (F) Western blot analysis of VCP expression in TPC-1 (NIS+ve) cells following treatment with 0.5 μM Ebastine, 0.25 μM Clotrimazole or 0.25 μM Astemizole. (G) Schematic indicating protocol for obtaining mouse thyrocytes. RAI uptake (H) and Western blot analysis (I) in mouse thyrocytes treated with 0.5 μM Ebastine (n=8) or 0.25 μM Clotrimazole (n=8). (J) RAI uptake in human thyrocytes treated as described with Ebastine or Clotrimazole at varying of doses of VCP inhibitors due to previous evidence of variability in VCP inhibitor sensitivity (50). *, $P<0.05$; **, $P<0.01$.

Figure 6. VCP and ARF4 expression associates with poorer survival and response to RAI. (*A*) ARF4 (left) and VCP (right) expression in normal thyroid and PTC in the THCA TCGA

dataset. (*B*) VCP expression in normal thyroid (*n*=12), PDTC (*n*=17) and ATC (*n*=20). (*C*) ARF4 (left) and VCP (right) expression in PTC with BRAF-like (*n*=272) or RAS-like genetic signatures (*n*=119). (*D*) ARF4 expression in PTC with indicated genetic alterations. (*E*) Frequency (%) of indicated genetic alterations in PTC with low (Q1Q2) versus high ARF4 (Q3Q4) expression. (*F-G*) Same as (*D-E*) but for VCP expression. (*H-J*) DFS for THCA with high (Q3Q4; >12.71) versus low (Q1Q2; <12.71) VCP expression for the entire PTC cohort (*H*), RAI-treated patients (*I*) and non-RAI treated patients (*J*). (*K*) Hazard ratios ±95% CI for patients stratified on median VCP and ARF4 tumoral expression in THCA with the indicated treatment and genetic signature or alteration. (*L-M*) DFS for THCA with high (Q3Q4; >11.84) versus low (Q1Q2; <11.84) ARF4 expression for RAI-treated PTC patients (*L*) and non-RAI treated PTC patients (*M*). NS, not significant; *, $P<0.05$; **, $P<0.01$; ***, $P<0.001$.

Figure 7. Putative model of NIS trafficking. NIS maintains a delicate balance between protein synthesis, folding, assembly, trafficking and degradation. (*i*) We propose NIS is glycosylated in the ER and upon correct folding transported to the Golgi. (*ii*) Protein surveillance pathways exist that target NIS for ERAD. As VCP does not require ATPase activity to inhibit NIS function, it is likely VCP acts to unfold NIS (*iii*) prior to proteasomal degradation. (*iv*) ARF4 recognizes the VAPK motif in the NIS C-terminus and promotes vesicular trafficking to the PM, where NIS is active (*v*). (*vi*) PBF has a YARF endocytosis motif and acts to bind and internalize NIS away from the PM in a clathrin-dependent process. (*vii*) Although inhibition of recycling by Dynasore suggests that ARF4 shuttles NIS to the PM, other proteins must promote recycling of NIS to the PM as with most PM transporters.

Figure 1

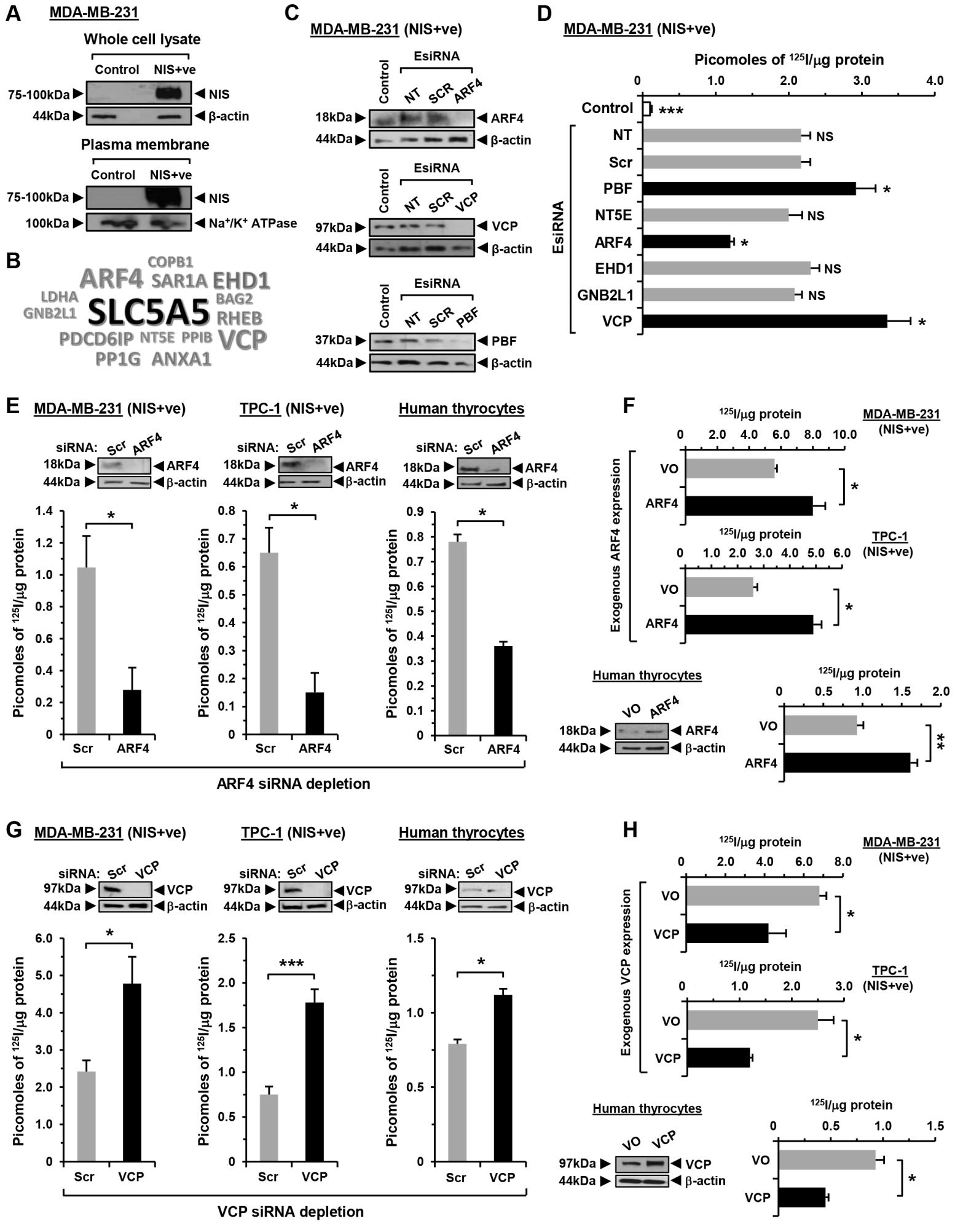
A
MDA-MB-231
Whole cell lysate
Control
NIS+ve
75-100kDa
NIS
44kDa
β-actin
Plasma membrane
Control
NIS+ve
75-100kDa
NIS
100kDa
Na+/K+ ATPase
B
COPB1
ARF4
SAR1A
EHD1
LDHA
BAG2
GNB2L1
SLC5A5
RHEB
PDCD6IP
NT5E
PPIB
VCP
PP1G
ANXA1
C
MDA-MB-231 (NIS+ve)
EsiRNA
Control
NT
SCR
ARF4
18kDa
ARF4
44kDa
β-actin
EsiRNA
Control
NT
SCR
VCP
97kDa
VCP
44kDa
β-actin
EsiRNA
Control
NT
SCR
PBF
37kDa
PBF
44kDa
β-actin
D
MDA-MB-231 (NIS+ve)
Picomoles of 125I/μg protein
0
1.0
2.0
3.0
4.0
Control
***
EsiRNA
NT
NS
Scr
PBF
*
NT5E
NS
ARF4
*
EHD1
NS
GNB2L1
NS
VCP
*
E
MDA-MB-231 (NIS+ve)
TPC-1 (NIS+ve)
Human thyrocytes
siRNA:
Scr
ARF4
18kDa
ARF4
44kDa
β-actin
Picomoles of 125I/μg protein
Scr
ARF4
ARF4 siRNA depletion
F
MDA-MB-231 (NIS+ve)
TPC-1 (NIS+ve)
Human thyrocytes
125I/μg protein
Exogenous ARF4 expression
VO
ARF4
*
**
18kDa
ARF4
44kDa
β-actin
G
MDA-MB-231 (NIS+ve)
TPC-1 (NIS+ve)
Human thyrocytes
siRNA:
Scr
VCP
97kDa
VCP
44kDa
β-actin
Picomoles of 125I/μg protein
Scr
VCP
VCP siRNA depletion
H
MDA-MB-231 (NIS+ve)
TPC-1 (NIS+ve)
Human thyrocytes
125I/μg protein
Exogenous VCP expression
VO
VCP
*
97kDa
VCP
44kDa
β-actin

Figure 2

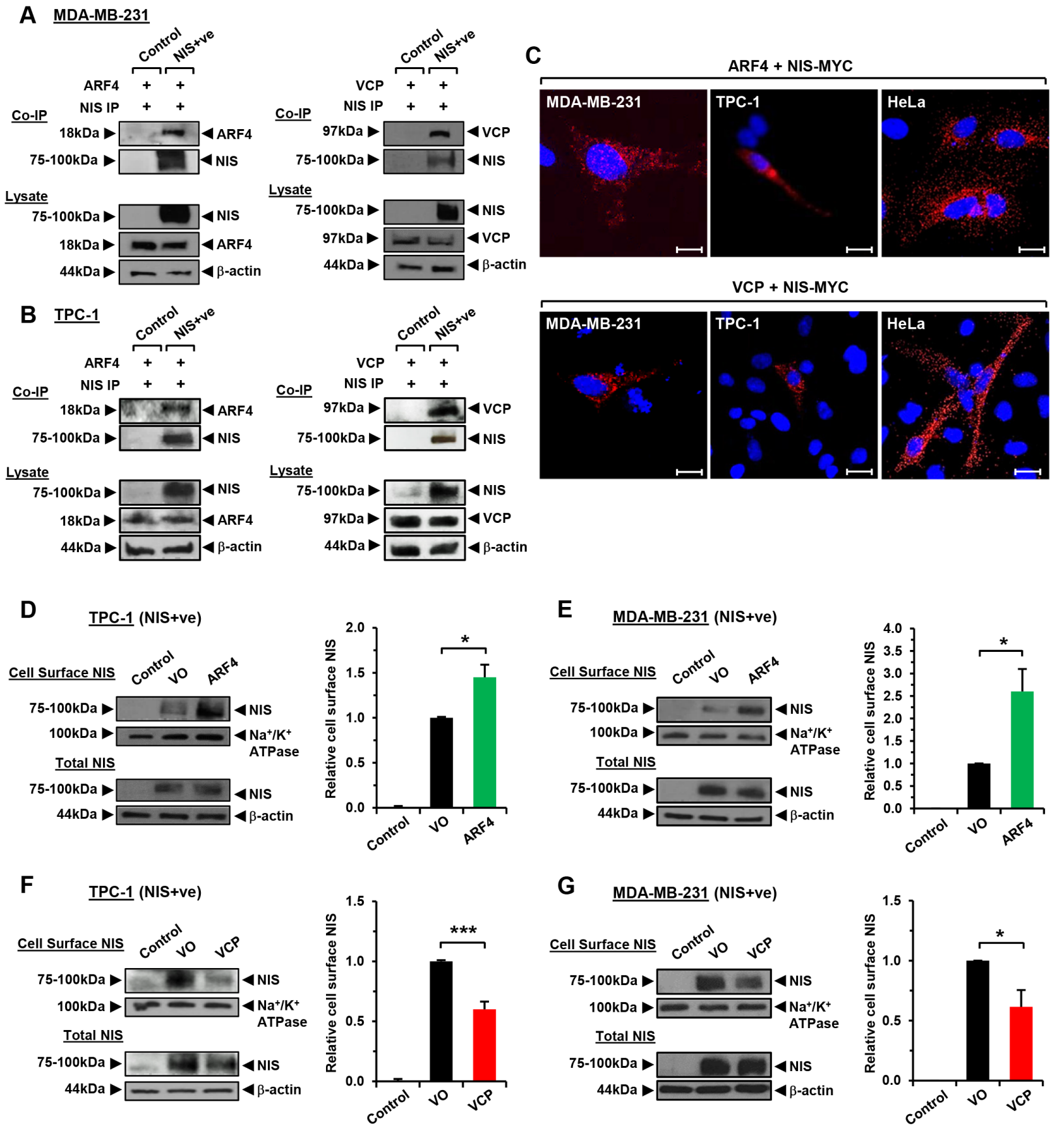
A
MDA-MB-231
Control
NIS+ve
ARF4
NIS IP
Co-IP
18kDa
75-100kDa
ARF4
NIS
Lysate
44kDa
β-actin
VCP
97kDa
B
TPC-1
C
ARF4 + NIS-MYC
VCP + NIS-MYC
MDA-MB-231
TPC-1
HeLa
D
TPC-1 (NIS+ve)
Cell Surface NIS
VO
Total NIS
100kDa
Na+/K+ ATPase
Relative cell surface NIS
E
MDA-MB-231 (NIS+ve)
F
TPC-1 (NIS+ve)
VCP
G
MDA-MB-231 (NIS+ve)

Figure 3

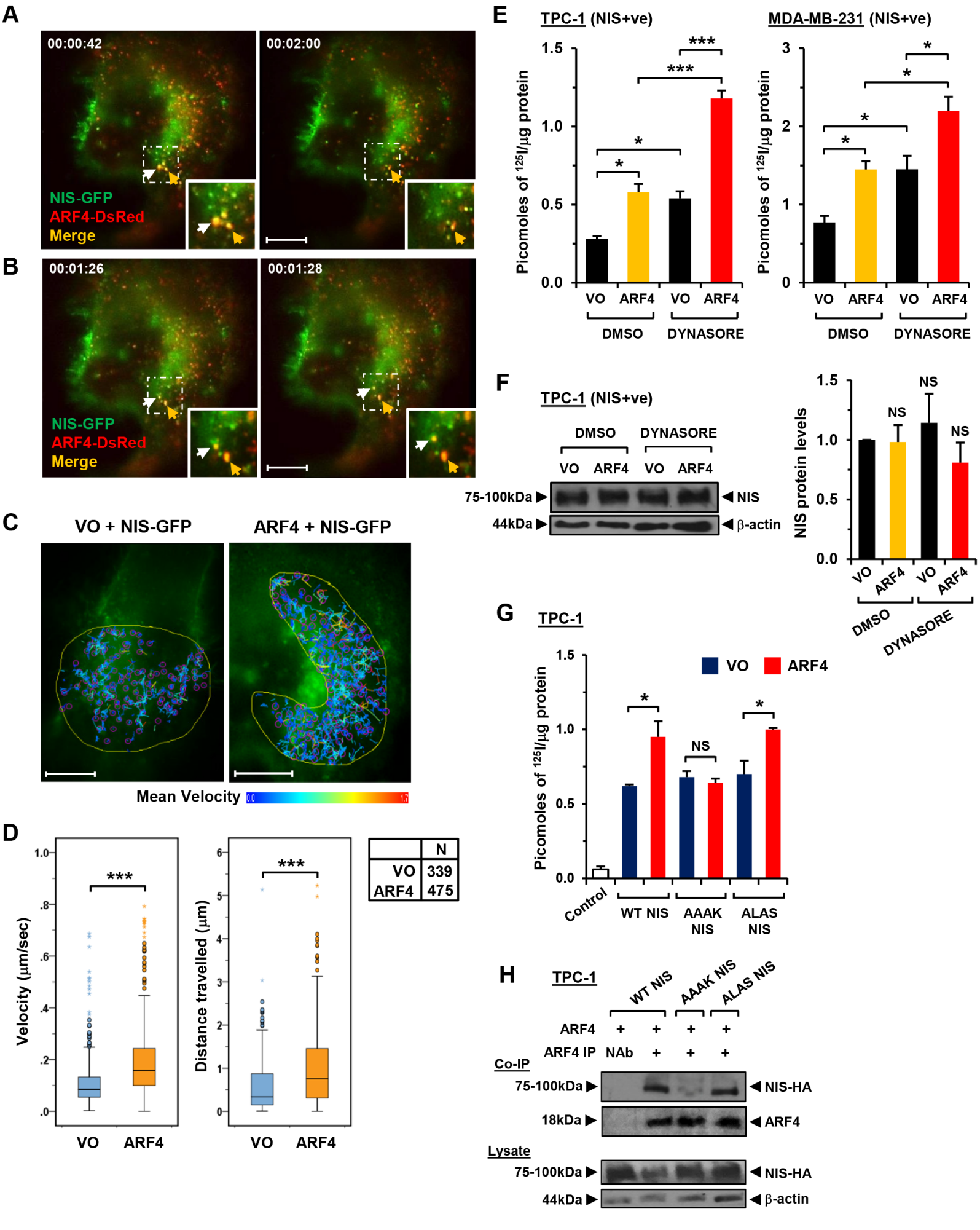
A
00:00:42
00:02:00
NIS-GFP
ARF4-DsRed
Merge
B
00:01:26
00:01:28
NIS-GFP
ARF4-DsRed
Merge
C
VO + NIS-GFP
ARF4 + NIS-GFP
Mean Velocity
D
Velocity (µm/sec)
Distance travelled (µm)
***
VO
ARF4
N
VO 339
ARF4 475
E
TPC-1 (NIS+ve)
MDA-MB-231 (NIS+ve)
Picomoles of 125I/µg protein
VO
ARF4
DMSO
DYNASORE
F
TPC-1 (NIS+ve)
DMSO
DYNASORE
75-100kDa
NIS
44kDa
β-actin
NIS protein levels
NS
G
TPC-1
VO
ARF4
Picomoles of 125I/µg protein
Control
WT NIS
AAAK NIS
ALAS NIS
H
TPC-1
WT NIS
AAAK NIS
ALAS NIS
ARF4
ARF4 IP
NAb
Co-IP
75-100kDa
NIS-HA
18kDa
ARF4
Lysate
75-100kDa
NIS-HA
44kDa
β-actin

Figure 4

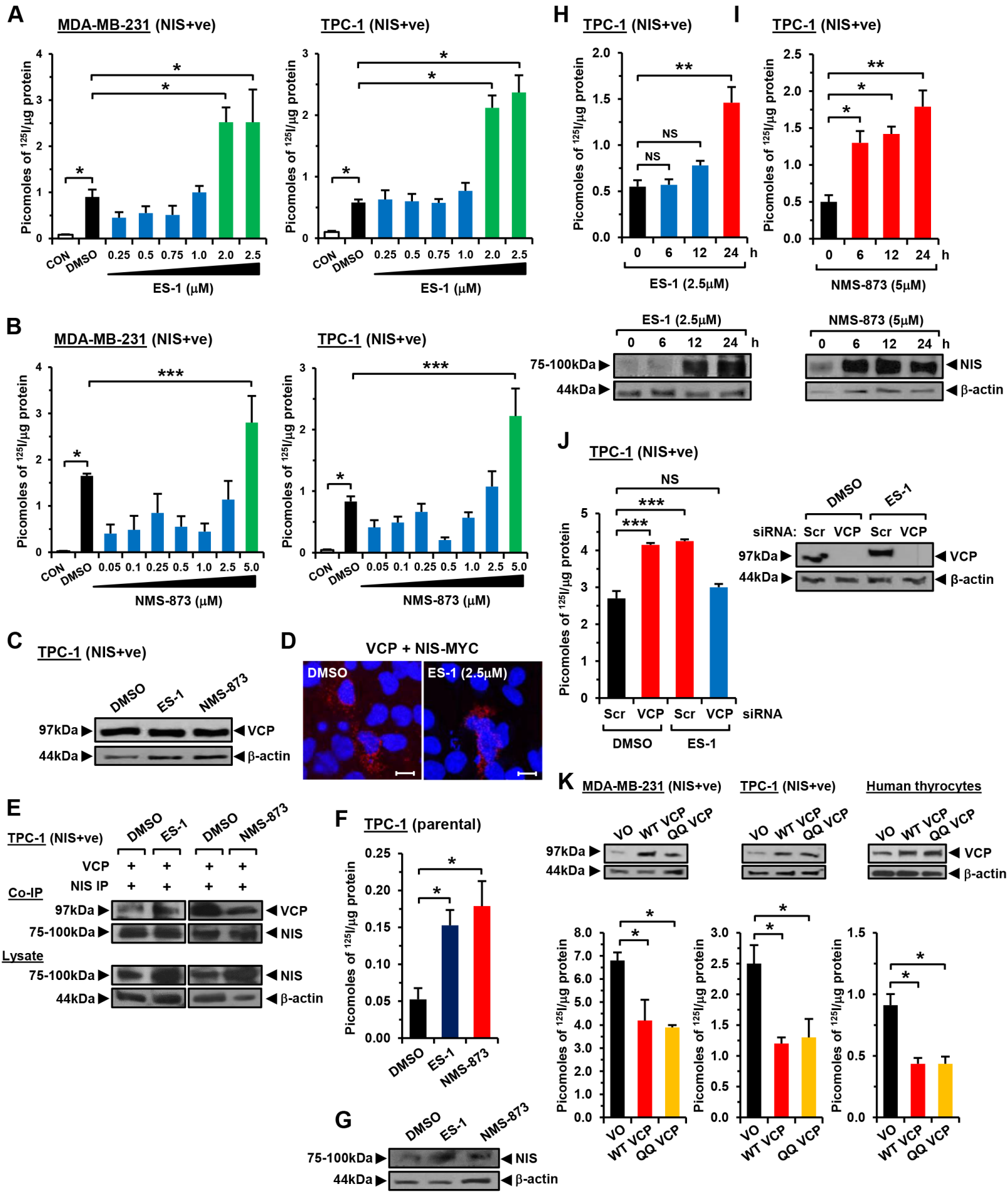
A
MDA-MB-231 (NIS+ve)
TPC-1 (NIS+ve)
Picomoles of 125I/µg protein
CON
DMSO
0.25 0.5 0.75 1.0 2.0 2.5
ES-1 (µM)
B
MDA-MB-231 (NIS+ve)
TPC-1 (NIS+ve)
CON
DMSO
0.05 0.1 0.25 0.5 1.0 2.5 5.0
NMS-873 (µM)
C
TPC-1 (NIS+ve)
DMSO
ES-1
NMS-873
97kDa
VCP
44kDa
β-actin
D
VCP + NIS-MYC
DMSO
ES-1 (2.5µM)
E
TPC-1 (NIS+ve)
DMSO
ES-1
DMSO
NMS-873
VCP
NIS IP
Co-IP
97kDa
VCP
75-100kDa
NIS
Lysate
75-100kDa
NIS
44kDa
β-actin
F
TPC-1 (parental)
Picomoles of 125I/µg protein
DMSO
ES-1
NMS-873
G
DMSO
ES-1
NMS-873
75-100kDa
NIS
44kDa
β-actin
H
TPC-1 (NIS+ve)
Picomoles of 125I/µg protein
NS
0 6 12 24 h
ES-1 (2.5µM)
I
TPC-1 (NIS+ve)
Picomoles of 125I/µg protein
0 6 12 24 h
NMS-873 (5µM)
ES-1 (2.5µM)
0 6 12 24 h
75-100kDa
44kDa
NMS-873 (5µM)
0 6 12 24 h
NIS
β-actin
J
TPC-1 (NIS+ve)
NS
Picomoles of 125I/µg protein
Scr VCP Scr VCP siRNA
DMSO
ES-1
DMSO
ES-1
siRNA: Scr VCP Scr VCP
97kDa
VCP
44kDa
β-actin
K
MDA-MB-231 (NIS+ve)
TPC-1 (NIS+ve)
Human thyrocytes
VO
WT VCP
QQ VCP
97kDa
VCP
44kDa
β-actin
Picomoles of 125I/µg protein
VO
WT VCP
QQ VCP

Figure 5

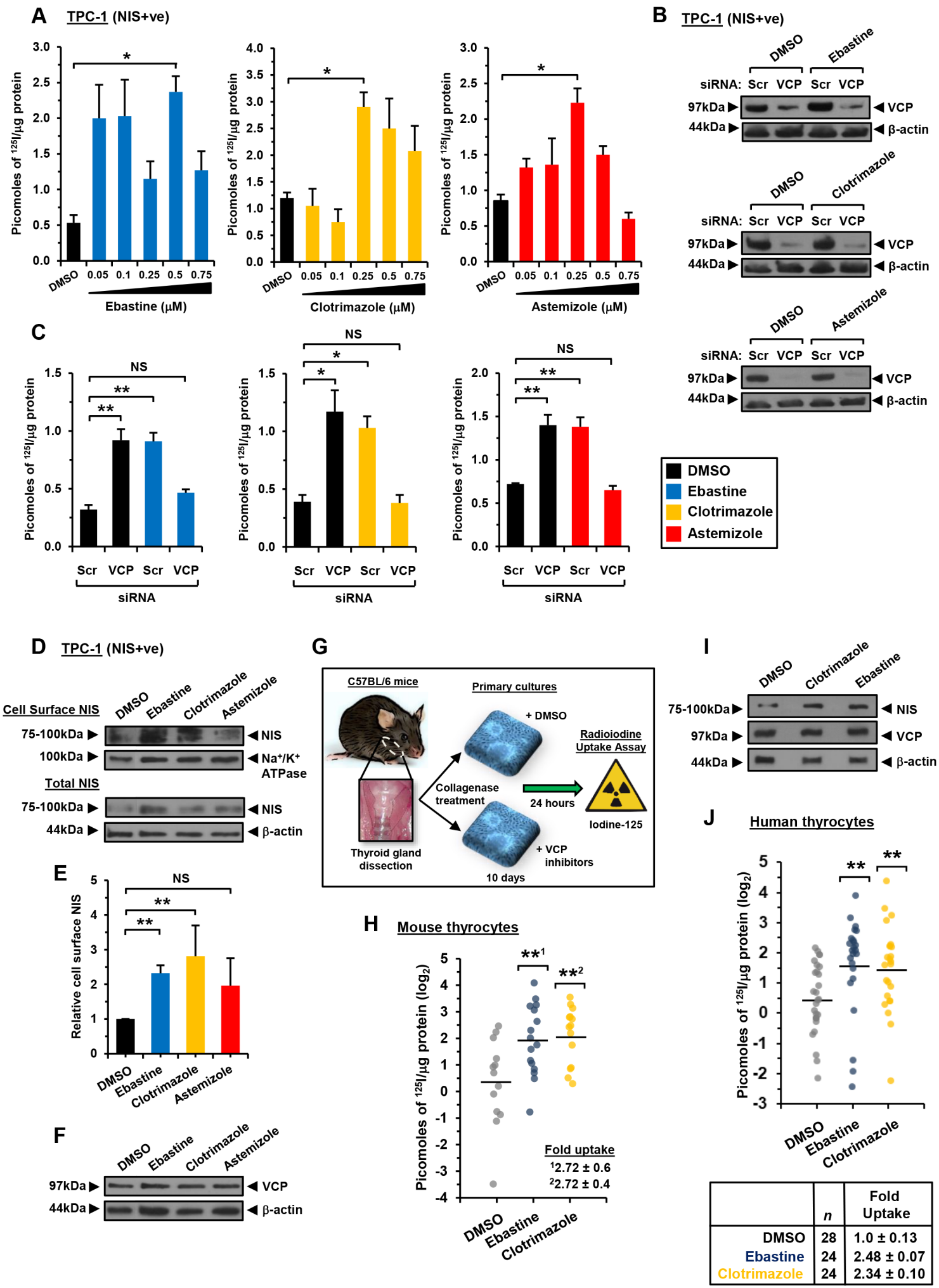

	n	Fold Uptake
DMSO	28	1.0 ± 0.13
Ebastine	24	2.48 ± 0.07
Clotrimazole	24	2.34 ± 0.10

Figure 6

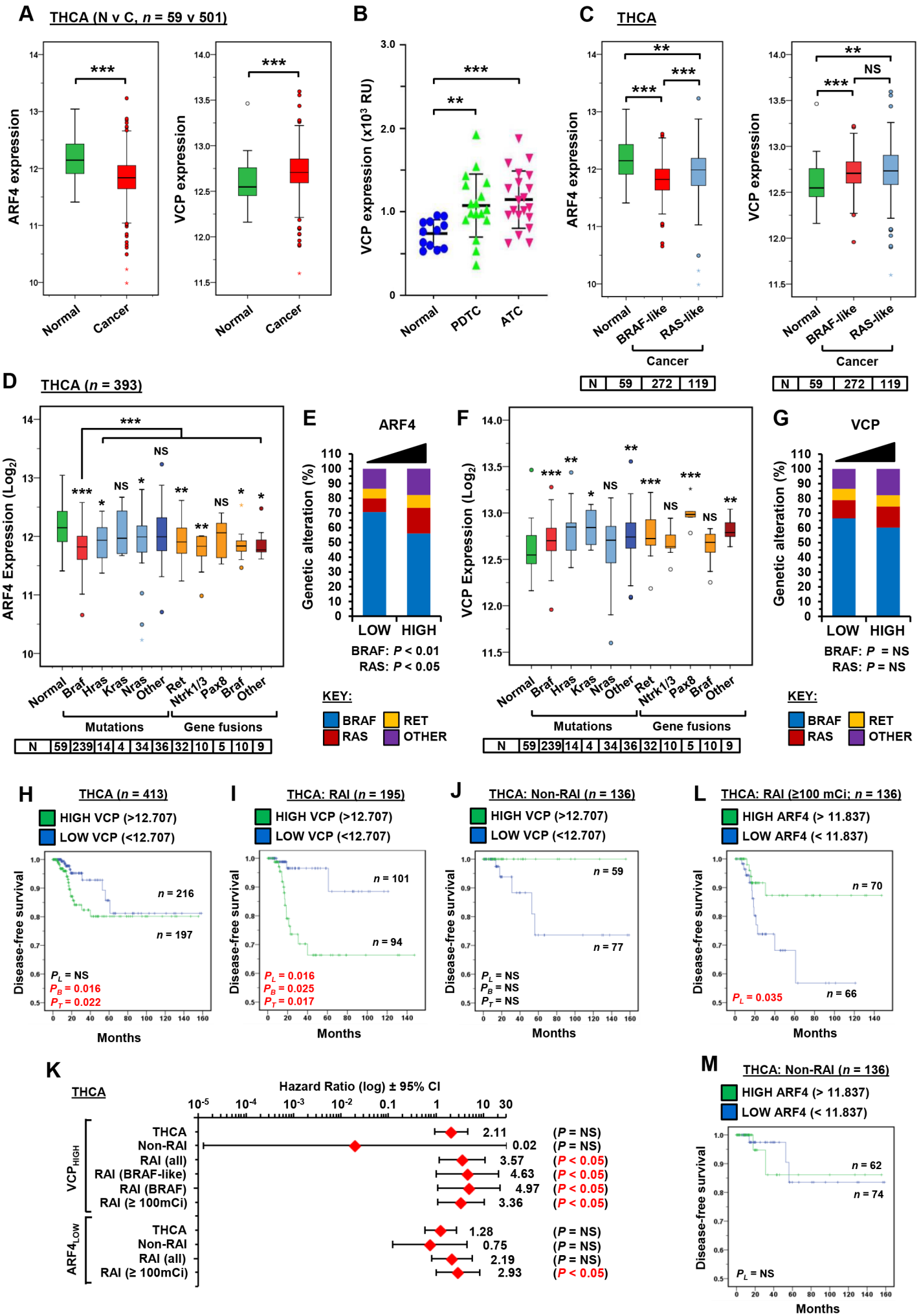
A
THCA (N v C, n = 59 v 501)
ARF4 expression
VCP expression
Normal
Cancer
B
VCP expression (x10³ RU)
Normal
PDTC
ATC
C
THCA
ARF4 expression
VCP expression
Normal
BRAF-like
RAS-like
Cancer
N 59 272 119
D
THCA (n = 393)
ARF4 Expression (Log2)
Normal Braf Hras Kras Nras Other Ret Ntrk1/3 Pax8 Braf Other
Mutations
Gene fusions
N 59 239 14 4 34 36 32 10 5 10 9
E
ARF4
Genetic alteration (%)
LOW HIGH
BRAF: P < 0.01
RAS: P < 0.05
KEY:
BRAF RET
RAS OTHER
F
VCP Expression (Log2)
Normal Braf Hras Kras Nras Other Ret Ntrk1/3 Pax8 Braf Other
Mutations
Gene fusions
N 59 239 14 4 34 36 32 10 5 10 9
G
VCP
Genetic alteration (%)
LOW HIGH
BRAF: P = NS
RAS: P = NS
KEY:
BRAF RET
RAS OTHER
H
THCA (n = 413)
HIGH VCP (>12.707)
LOW VCP (<12.707)
n = 216
n = 197
PL = NS
PB = 0.016
PT = 0.022
Disease-free survival
Months
I
THCA: RAI (n = 195)
HIGH VCP (>12.707)
LOW VCP (<12.707)
n = 101
n = 94
PL = 0.016
PB = 0.025
PT = 0.017
Disease-free survival
Months
J
THCA: Non-RAI (n = 136)
HIGH VCP (>12.707)
LOW VCP (<12.707)
n = 59
n = 77
PL = NS
PB = NS
PT = NS
Disease-free survival
Months
L
THCA: RAI (≥100 mCi; n = 136)
HIGH ARF4 (> 11.837)
LOW ARF4 (< 11.837)
n = 70
n = 66
PL = 0.035
Disease-free survival
Months
K
THCA
Hazard Ratio (log) ± 95% CI
VCP HIGH
THCA 2.11 (P = NS)
Non-RAI 0.02 (P = NS)
RAI (all) 3.57 (P < 0.05)
RAI (BRAF-like) 4.63 (P < 0.05)
RAI (BRAF) 4.97 (P < 0.05)
RAI (≥ 100mCi) 3.36 (P < 0.05)
ARF4 LOW
THCA 1.28 (P = NS)
Non-RAI 0.75 (P = NS)
RAI (all) 2.19 (P = NS)
RAI (≥ 100mCi) 2.93 (P < 0.05)
M
THCA: Non-RAI (n = 136)
HIGH ARF4 (> 11.837)
LOW ARF4 (< 11.837)
n = 62
n = 74
PL = NS
Disease-free survival
Months

Figure 7

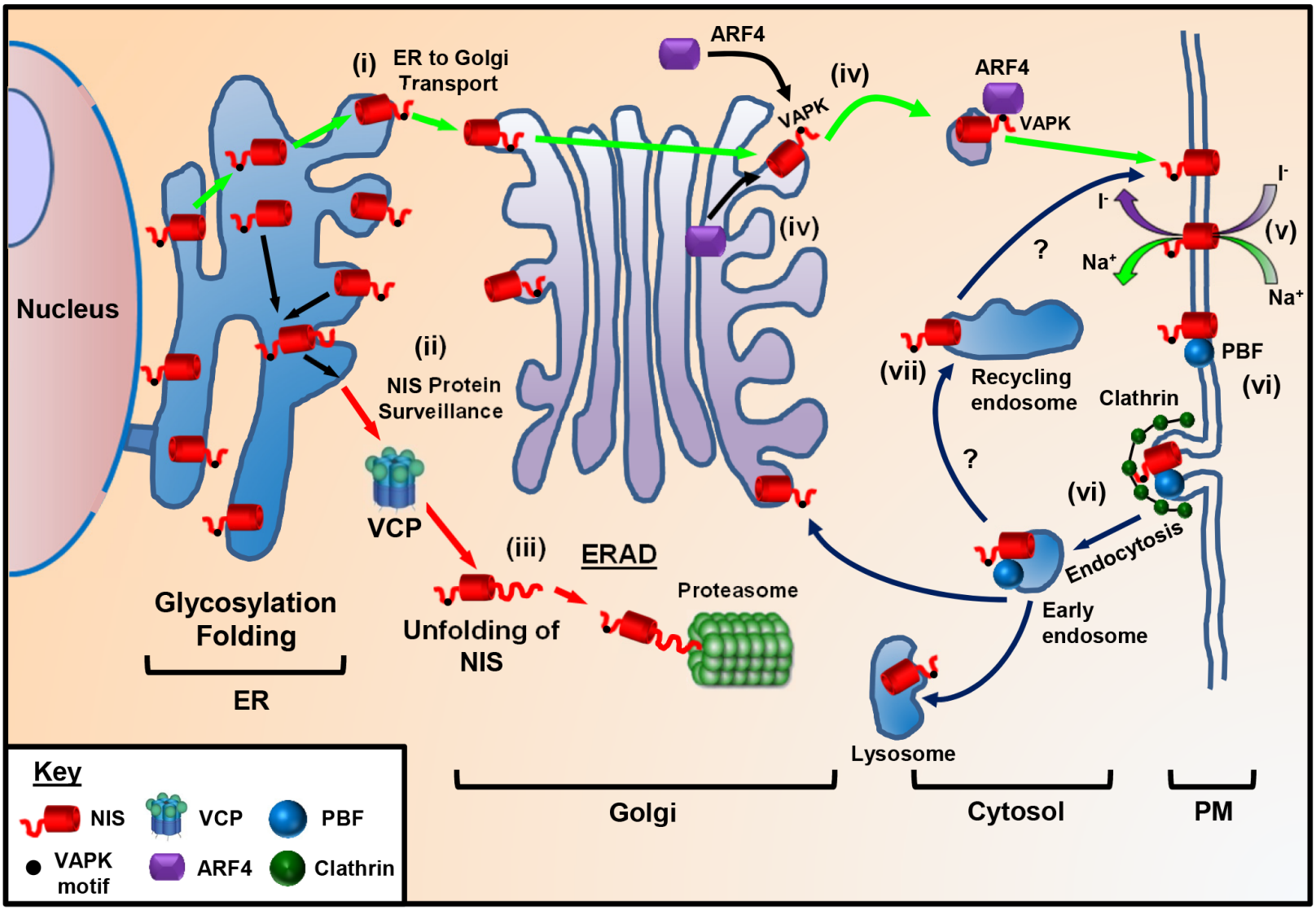
Nucleus
(i) ER to Golgi Transport
ARF4
VAPK
(iv)
ARF4
VAPK
(iv)
I-
I-
(v)
Na+
Na+
?
(ii)
NIS Protein Surveillance
(vii)
Recycling endosome
PBF
(vi)
Clathrin
VCP
?
(vi)
Endocytosis
(iii)
ERAD
Proteasome
Glycosylation Folding
Unfolding of NIS
Early endosome
Lysosome
ER
Golgi
Cytosol
PM
Key
NIS
VCP
PBF
VAPK motif
ARF4
Clathrin